J. Phys.: Condens. Matter **23** (2011) 000000 (8pp) UNCORRECTED PROOF

Electron localization and magnetism in $SrRuO_3$ with non-magnetic cation substitution

Q.1 **W Tong[1,2], F-Q Huang[1] and I-W Chen[3]**

[1] Shanghai Institute of Ceramics, Chinese Academy of Sciences, Shanghai 200050, People's Republic of China
[2] High Magnetic Field Laboratory, Chinese Academy of Sciences, Hefei, Anhui 230031, People's Republic of China
[3] Department of Materials Science and Engineering, University of Pennsylvania, Philadelphia, PA 19104-6272, USA

E-mail: weitong@hmfl.ac.cn

Received 29 October 2010, in final form 24 December 2010
Published
Online at stacks.iop.org/JPhysCM/23/000000

(*Abs. Ed: Emily*)
Processing/JPCM/
cm373761/PAP
Printed 1/2/2011
Spelling US
Issue no
Total pages
First page
Last page
File name
Date req
Artnum
Cover date

Abstract

Q.2 The destruction of the ferromagnetism of alloyed $SrRuO_3$ can be caused by electron localization at the substitution sites. Among all the non-magnetic cations that enter the B site, Zr^{4+} is the least disruptive to conductivity and ferromagnetism. This is because Zr^{4+} does not cause any charge disorder, and its empty d electron states which are poorly matched in energy with the Ru t_{2g}^4 states cause the least resonance scattering of Ru's d electrons. Conducting $Sr(Ru, Zr)O_3$ may be used as an electrode for perovskite-based thin film devices, while its insulating counterpart provides unprecedented magnetoresistance, seldom seen in other non-manganite and non-cobaltite perovskites.

Q.3 (Some figures in this article are in colour only in the electronic version)

1. Introduction

Strontium ruthenate $SrRuO_3$ with its unusually high Curie temperature (T_C) of 160 K is practically the only ferromagnetic (FM) metal among 4d transition metal oxides [1]. It is generally believed that the magnetism in this ABO_3 perovskite is of the Stoner type, arising from a high density of state (DOS) at the Fermi level (E_f) due to a nearby van Hove singularity [2]. The DOS of $SrRuO_3$ indeed has a sharp peak that nearly coincides with E_f according to the band structure calculation of Mazin and Singh [2]. A-site substituted $Sr_{1-x}Ca_xRuO_3$ is also metallic despite a substantial lattice contraction with Ca substitution [3, 4]. FM is maintained up to $x = 0.8$, but $CaRuO_3$ is paramagnetic—although its DOS is highly elevated at E_f, it has a relatively flat top which makes $CaRuO_3$ less susceptible to Stoner instability. On the other hand, nearly all alloying efforts attempting to fine tune the DOS by modifying lattice distortions severely suppress the FM [4–12]. This includes A-site substitution of either undersized cations (Ca, La/Na) or oversized cations (La/K, Pb) [4, 12]. In fact, $Sr_{1-x}La_{x/2}Na_{x/2}RuO_3$ loses FM faster than $Sr_{1-x}Ca_xRuO_3$ despite a smaller lattice contraction, indicating a strong FM-suppressing effect of A-site disorder [4]. However, a significantly higher T_C is found in $Sr(Ru_{1-x}Cr_x)O_3$ [9], making this a rather exceptional case whose origin is still under investigation [13–20].

One consequence of a high DOS at E_f is a large magnetic susceptibility, which causes a magnetic impurity to induce a giant magnetic moment around it. This effect, well known in nearly FM Pd in which 3d magnetic impurities induce a large host polarization [21, 22], was also theoretically predicted for $SrRuO_3$ and $CaRuO_3$ [2], the latter on the verge of FM. Experimental evidence of a giant magnetic moment was observed in $SrRuO_3$ doped with Fe and Co impurities, both causing an increase in magnetization [5, 6]. These impurities generate an especially strong effect because their empty orbitals at t_{2g} levels are energetically close to Ru's partially filled t_{2g} level, allowing electron resonance between impurities and Ru^{4+}, hence spin polarization of the neighboring electrons.

In view of the complexity of these alloys, we believe that to fully understand the dopant effects in $SrRuO_3$ and $CaRuO_3$ it would be necessary to turn to simpler models

Table 1. Nominal valence and ionic radii of non-magnetic B-site cations, compared to Ru^{4+} with an ionic radius of 62 pm. Also listed are critical concentrations x_c for the metal/insulator transition in substituted $SrRu_{1-x}B'_xO_3$ samples.

B'	Li	Mg	Zn	Sc	Lu	Ti	Zr	Nb
Valence	+1	+2	+2	+3	+3	+4	+4	+5
Radii (pm)	76	72	74	74.5	86	60.5	72	64
x_c	<0.1	<0.1	0.10	0.21	0.10	0.31	0.28	0.13

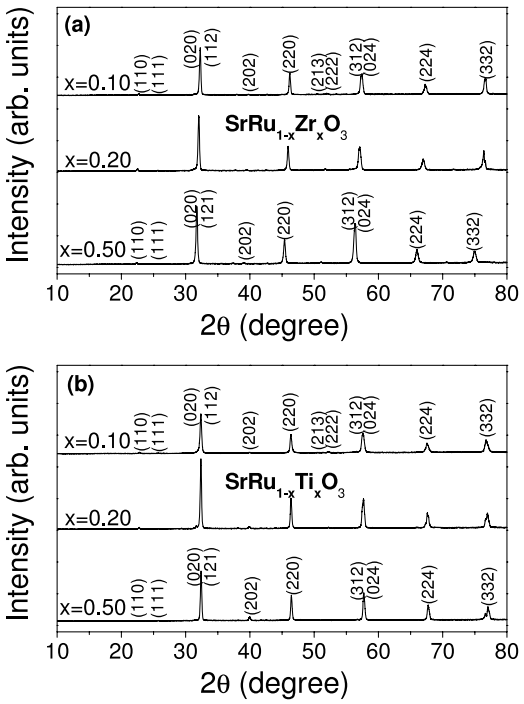

Figure 1. X-ray diffraction patterns of (a) $SrRu_{1-x}Zr_xO_3$ and (b) $SrRu_{1-x}Ti_xO_3$ ($x = 0.10$, 0.20 and 0.50) ceramics, pulverized. The indexing is based on PDF card 79-735.

focusing on non-magnetic impurities, i.e, impurities with a d^0 electronic configuration. In the past, this has been rarely done except for A-site dopants. One reference point that may be used to view the effects of non-magnetic B-site dopants is the Jaccarino–Walker model [23], which was developed for metallic alloys that suffer a sudden loss of the FM moment when the FM site loses a critical number of FM nearest neighbors. In the following it will be shown that this model does not apply to $SrRuO_3$; instead, the deterioration of FM upon B-site substitution proceeds by way of Anderson localization of itinerant electrons. The current work also reveals the best strategy to obtain highly conductive $SrRuO_3$ alloys that may be used as an electrode for perovskite-oxide-based devices [24–26].

2. Experimental procedures

Polycrystalline ceramic samples of the compositions $SrRu_{1-x}B'_xO_3$, with x up to 0.55 for Zr and Ti, 0.5 for Sc and Lu, 0.33 for Mg and Zn, 0.25 for Li and Nb, were prepared with starting materials of $SrCO_3$, RuO_2, and various oxides of B'. In the above B' (Li, Mg, Zn, Sc, Lu, Ti, Zr and Nb), none contains any d electron in its most common, ionized states. The valences (z) and the Shannon cation radii in the six-fold coordination [27] of these B' are listed in table 1; they cover a very broad range of sizes and valences. (In table 1, the composition of metal/insulator transition is also listed, to be discussed later.) Certain combined A-site and B-site substitutions $Sr_{1-x}A_xRu_{1-x}B'_xO_3$ (e.g., La_2Mg meaning the composition of $Sr_{1-2x}La_{2x}Ru_{1-x}Mg_xO_3$), using A = La and B′ = Mg, Sc, Ti or Zr, were also investigated.

Sintering was performed in air at 1200–1500 °C with samples embedded inside a powder pack to minimize Ru evaporation. Phase purity was monitored with x-ray powder diffraction (XRD) using Cu K_α radiation, with Si powder added as an internal standard, to ensure only single-phase perovskite samples were used for further studies. Additional verification of phase purity and compositional uniformity was provided by elemental mapping using an electron microprobe. Magnetization (M) and (four-point-probe) electrical conductivity ($\sigma = \rho^{-1}$) were measured using a Physical Property Measurement System (Quantum Design PPMS) at various magnetic fields (H) up to 90 kOe between 10 and 300 K. Other experimental details were similar to those described elsewhere [5, 6].

3. Results

3.1. Phase purity and structure

Since only single-phase perovskite samples are suitable for evaluating the dopant effects, we verified their phase purity using several techniques. Shown in figure 1 are the XRD patterns of $Sr(Ru_{1-x}Zr_x)O_3$ and $Sr(Ru_{1-x}Ti_x)O_3$, in which all the peaks can be indexed using perovskite reflections (orthorhombic, *Pbnm* $GdFeO_3$ structure in this case), indicating the absence of impurity phases. This example is chosen because Zr and Ti doping will prove to be the least disruptive to FM and electrical conductivity. Figure 2 shows the variation of unit cell volume versus x for Lu, Sc, Zr, Ti and Nb, all of which produced single-phase diffraction patterns at lower x (up to $x = 0.5$ for Lu and Sc, 0.55 for Zr and Ti, and 0.2 for Nb; data not shown). The systematic variation from undersized Ti^{4+}, to oversized Zr^{4+} and Lu^{3+} is indicative of the incorporation of the dopants into the lattice. These data also provide evidence for the variation of Ru's ionic state under $z \neq 4$ doping: for slightly oversized Nb^{5+}, the cell volume increases presumably because of Ru^{4+} reduction to the larger sized Ru^{3+}; conversely, although Sc^{3+} is slightly larger than Zr^{4+}, it causes less cell volume expansion presumably because of Ru^{4+} oxidation to the smaller sized Ru^{5+}. In figure 3, the fractography, electron diffraction pattern and elemental mapping of a $Sr(Ru_{0.5}Zr_{0.5})O_3$ sample are shown to illustrate

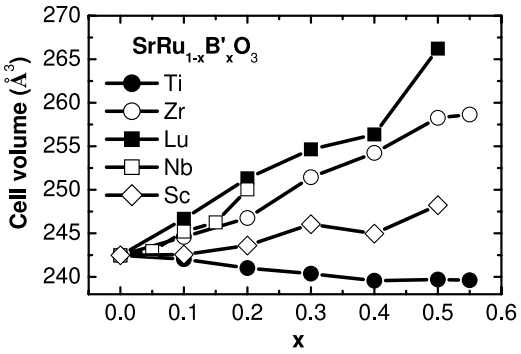

Figure 2. Unit cell volume versus x for several dopants, to illustrate the range of their solubilities (lower for Nb but comparable for Sc, Lu, Ti and Zr) and size/charge effects.

the uniformity of the microstructure and composition in this sample.

3.2. Magnetism

Both magnetic properties (M, T_C, etc) and conductivity were found to monotonically decrease with increasing x. Examples of the suppression of magnetization by substitutions are provided in figure 4 for several substitutions at two fields and at $x = 0.1$ and 0.2, which are well within the respective solubility limits. All the $M(T)$ measurements shown here were carried out during field-cooling. As extensively documented in previous studies of $Sr_{1-x}La_xRu_{1-x}Fe_xO_3$ and $Sr_{1-x}La_xRu_{1-x}Co_xO_3$ [5, 6], with increasing x FM is replaced by magnetic characteristics reminiscent of cluster glass and spin glass. Similar property evolutions were also observed for all substitutions studied here, and they will not be elaborated further. However, it should be emphasized that different B-site dopants have rather different effects on FM despite their similar d^o configuration. Some, such as Zr, Ti and Sc, cause a relatively small decrease in M and T_C, while others, such as Li and Mg, strongly depress both M and T_C even at $x = 0.1$. This is at odds with the Jaccarino–Walker model [23].

The field (H) dependence of magnetization at 10 K is depicted in figure 5 for all the Zr and Ti doped samples. The magnetization is progressively suppressed with x, which agrees with the M–T results. At the lowest x level (0.1), the saturation magnetization was decreased for Ti doping but not for Zr doping. At the highest x levels (0.5 and 0.55), the magnetization under Ti doping—but not under Zr doping—becomes almost linear with H indicating the complete destruction of the FM order. These data suggest that $SrRu_{1-x}Zr_xO_3$ retains more FM than $SrRu_{1-x}Ti_xO_3$ at the same x.

3.3. Conductivity

With increasing x, the metallic conductivity of $SrRuO_3$ gradually crossovers to a semiconducting/insulating behavior in substituted alloys. This is illustrated in figure 6 for several substitutions at $x = 0.1$ and 0.2. To aid comparison, the resistivity ρ as a function of temperature (T) is normalized by its value at 300 K, $\rho_{300\,K}$. Two features are noteworthy

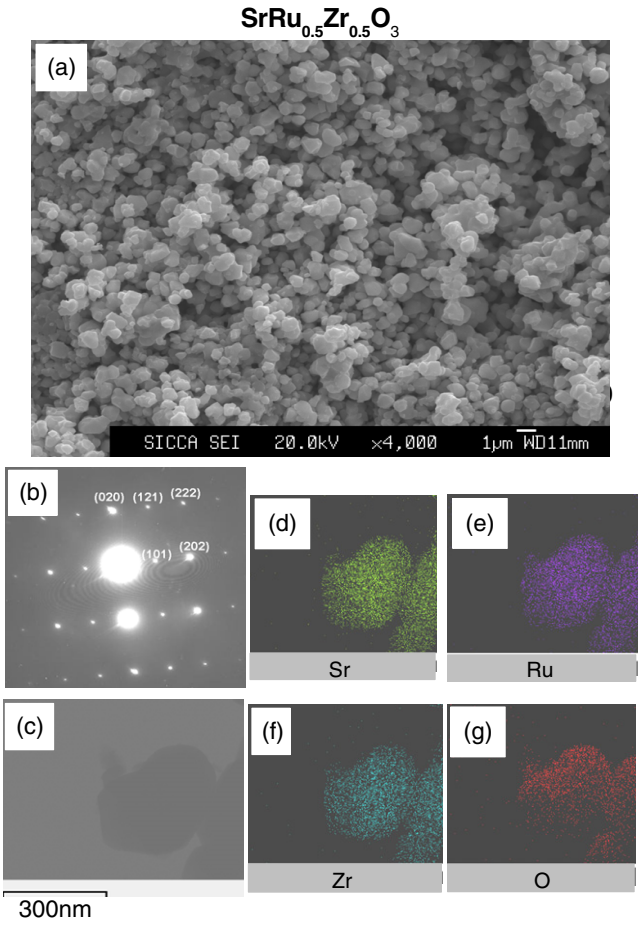

Figure 3. (a) Scanning electron micrograph of fractured $SrRu_{1-x}Zr_xO_3$ ceramic, at $x = 0.5$, (b) transmission electron microscope (TEM) selected area electron diffraction pattern for the grain shown in (c); (d)–(g) are the elemental mapping of the same grain for Sr, Ru, Zr, and O, respectively. The indexing in (b) is based on PDF card 79-735.

and illustrated for $Sr(Ru_{0.8}Zr_{0.2})O_3$ in the inset of figure 6(b). First, there is a characteristic kink at the temperature that corresponds to the T_C in figure 4. This was observed in figure 6 in the $\rho(T)/\rho_{300\,K}$ plots for Zr, Ti, and Sc substitutions. Such kink is well known to be due to the scattering of itinerant electrons by enhanced critical spin fluctuations near T_C [28]. Second, at $x = 0.1$, all except Li shows a minimum resistivity at an intermediate temperature before an upturn, as 0 K is approached. The temperature of the resistivity minimum is higher at $x = 0.2$ than at $x = 0.1$. This behavior, which has also been commonly seen in other studies of $SrRuO_3$ [29] and its alloys (e.g., [5, 6, 9]), is characteristic of Anderson disorder in metals, in which the resistivity rises at the low temperature due to a weak localization contribution. (At such low temperature, the mean free path of electrons exceeds Anderson's localization length for electrons, triggering the localization effect.) A further manifestation of this behavior, illustrated in figure 7(a) for Sc substitution, is a crossover of the higher temperature slope from a positive $d\rho/dT$ (metal-like) at $x \leqslant 0.1$, to nearly $d\rho/dT = 0$ at $x = 0.2$ (barely metal-like with a very slightly positive slope at higher temperature), then to a negative $d\rho/dT$ (insulator-like) at

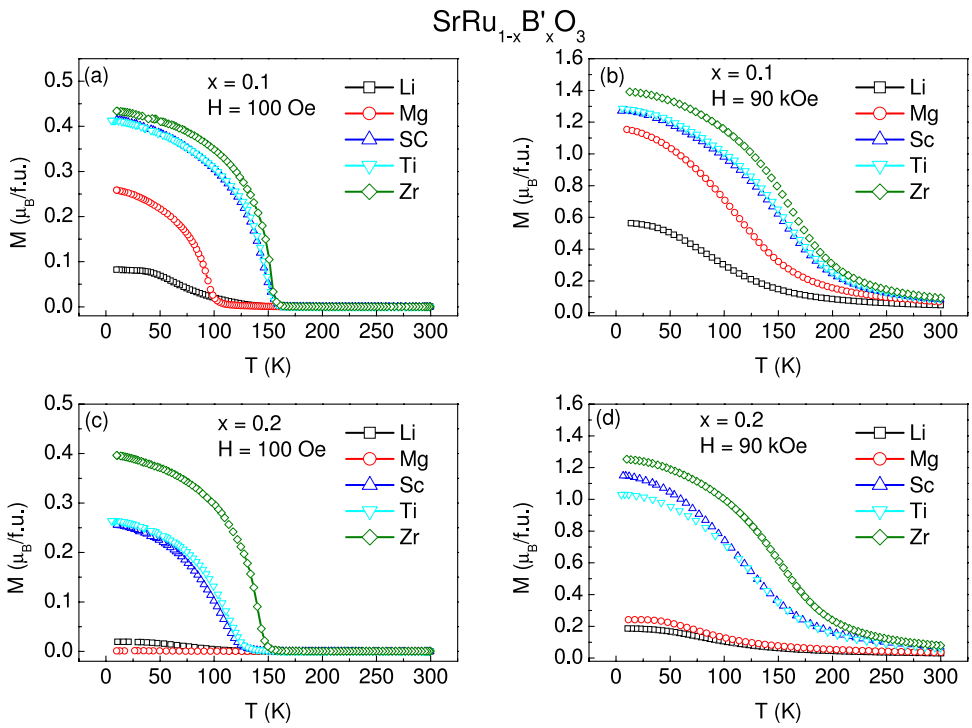

Figure 4. $M(T)$ curves at 100 Oe and 90 kOe for Li, Mg, Sc, Ti and Zr substituted $SrRu_{1-x}B'_xO_3$ samples, at $x = 0.1$ ((a), (b)) and 0.2 ((c), (d)). (One formula unit f.u. per conventional pseudocubic unit cell.).

$x = 0.3$, indicating a metal-to-insulator transition. A similar transition is seen in figure 7(b) for Nb substitution, occurring between $x = 0.1$ and 0.15. We have estimated the transition compositions x_c (where $d\rho/dT = 0$) by interpolation and, as shown in table 1, this transition occurs at $x_c \sim 0.3$ for Zr and Ti, at ∼0.2 for Sc, 0.13 for Nb, 0.1 for Zn and Lu, and <0.1 for Li and Mg. Again, as in their effects on M and T_C, different substitutions have greatly different suppressing effects on metallicity. Some, such as Zr and Ti, cause a relatively small decrease in metallicity and has a relatively large x_c, while others, such as Li and Mg, strongly depress metallicity and x_c.

3.4. Correlation between magnetic and transport properties

Comparing the effects on M, T_C, $\rho(T)/\rho_{300\ K}$ and x_c, we find a new, broad picture to reveal itself: there is a strong correlation between the magnetic and transport properties. To illustrate this correlation, we first compare for various compositions the normalized conductivity ($\sigma_{20\ K}/\sigma_{300\ K}$ and $\sigma_{60\ K}/\sigma_{300\ K}$) with the 'saturation' magnetization $M_{90\ kOe}$ (measured at 10 K) and the 'weak-field' magnetization $M_{100\ Oe}$ (measured at either 10 K or T_f—the freezing temperature of spin-glass-like samples). They are strongly correlated as shown in figure 8 for both $x = 0.1$ and 0.2. Note that a small value of normalized σ is indicative of Anderson localization as already illustrated in figures 6 and 7. Note further that in figure 8, the samples of the B-site substitution are arranged in the order of increasing nominal valence z of the B' cation, $Li^+ < Mg^{2+} = Zn^{2+} < Sc^{3+} = Lu^{3+} < Ti^{4+} = Zr^{4+} < Nb^{5+}$. It is then seen that the B' that is the least disruptive to FM and electron delocalization has $z = 4$ or 3, such as Zr^{4+}, Ti^{4+} and Sc^{3+}, whereas the disruption increases when z deviates from these values and is especially severe for Li^+ and Mg^{2+}. Since dopants other than Ti^{4+} and Zr^{4+} are likely to cause a change in the valence state of Ru^{4+}, this electronic (band filling/emptying) effect along with the charge disorder effect is apparently most deleterious to both FM and metallicity.

It is further found that simultaneous A- and B-site substitution often disrupts FM and causes more localization. For example, the (La, Sc), (La, Ti) and (La, Zr) combinations in figure 8 have a lower M and a lower normalized σ than the alloys substituted by Sc, Ti and Zr alone. This is reminiscent of the A-site disorder effect mentioned in section 1. On the other hand, there is no overriding correlation with the size of the cations, which affects lattice distortion. According to table 1, the cationic radii in six-fold coordination follows $Ti^{4+} < Ru^{4+} < Nb^{5+} < Mg^{2+} = Zr^{2+} < Zn^{2+} < Sc^{3+} < Li^+ < Lu^{3+}$; the data in figure 8 do not follow such a sequence.

To further substantiate the correlation between magnetism and electron delocalization, we plot M versus the normalized σ in figure 9(a). The correlation is excellent for B-site substitutions (figure 9(a) for $x = 0.2$ and upper inset for $x = 0.1$); it is also quite good when combined A and B-site substitutions are considered (lower inset in figure 9(a)). A similar correlation between T_C and normalized conductivity is found for B-site substitutions (figure 9(b)) as well as combined A and B-site substitutions (inset in figure 9(b)). Since all these substituting cations are non-magnetic, they should have the same effect on FM according to the Jaccarino–Walker picture. This is evidently not the case here. Instead, there is no doubt that FM is corrupted by the localization of itinerant electrons since both M and T_C decrease with

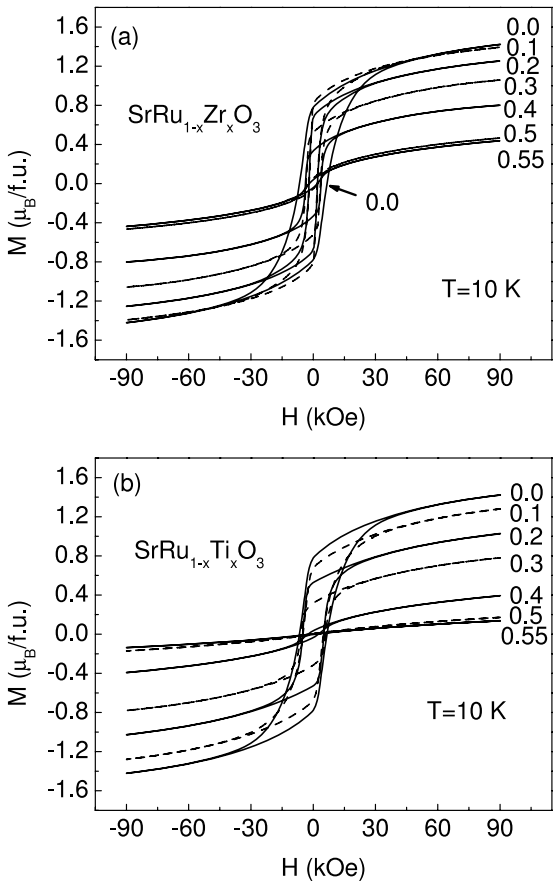

Figure 5. $M(H)$ loops at 10 K for (a) Zr and (b) Ti substituted $SrRu_{1-x}B'_xO_3$ samples (x = 0–0.55).

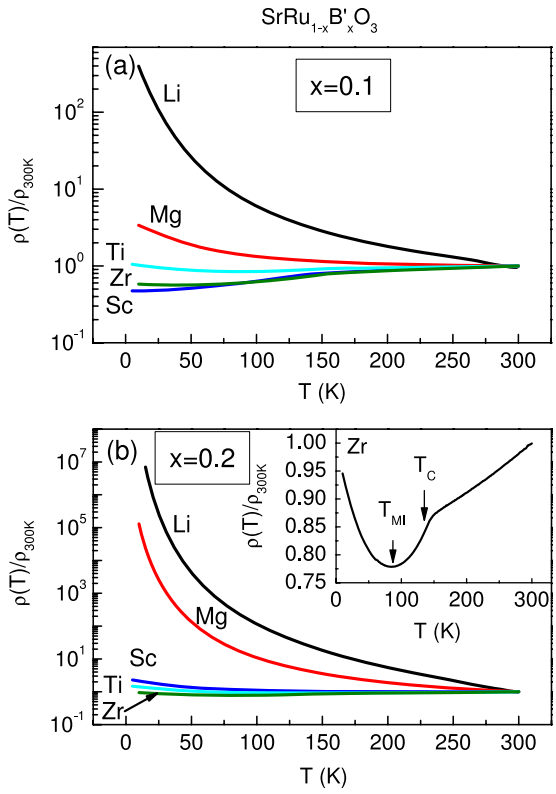

Figure 6. Normalized $\rho(T)$ curves for Li, Mg, Sc, Ti and Zr substituted $SrRu_{1-x}B'_xO_3$ samples, at x = 0.1 (a) and 0.2 (b). Inset in (b) shows detail near T_C and minimal resistivity for $SrRu_{0.8}Zr_{0.2}O_3$.

reduced conductivity, whereas FM can be largely sustained if metallicity is maintained.

The retention of metallicity and its interplay with Stoner FM was further addressed by the temperature dependence and field dependence of resistivity. Recall that there is a characteristic kink at T_C in magnetic metals due to the scattering of itinerant electrons by enhanced critical spin fluctuations. As shown in figure 10 for $Sr(Ru_{1-x}Zr_x)O_3$ this kink is suppressed by applying a large magnetic field (90 kOe), which suppresses spin fluctuations. This leads to a characteristic peak at T_C in the (negative) magnetoresistance (MR), defined as $\frac{\rho(T,H=90\text{ kOe})-\rho(T,H=0\text{ Oe})}{\rho(T,H=0\text{ Oe})}$, in figure 10 inset, which may be used as sensitive signature of magnetism. For $Sr(Ru_{1-x}Zr_x)O_3$, this peak persists at $x = 0.3$ ($T_C = 108.5$ K in figure 9, versus the MR peak at 112 K in figure 10 inset), despite the fact that the temperature dependence of $\rho(T)$ is no longer the metallic type (figure 10 main panel). This indicates that there are still itinerant electrons and critical spin fluctuations in this nominally insulating composition, i.e., a coexistence of (FM) metallic and insulating regions in this sample. In contrast, while a MR peak was also seen in $SrRu_{1-x}Ti_xO_3$ at x = 0–0.2, it disappeared from the $x = 0.3$ sample for Ti substitution and other non-Zr substitutions (data not shown). So the ability to sustain metallicity in heavily Zr substituted $SrRuO_3$ alloys is unmatched by any other non-magnetic dopant studied here. Incidentally, associated with the insulating behavior is another low temperature MR component that rises with decreasing temperature, as already reported in our previous work on $Sr_{1-x}La_xRu_{1-x}Fe_xO_3$, $Sr_{1-x}La_xRu_{1-x}Co_xO_3$, $Ca_{1-x}La_xRu_{1-x}Fe_xO_3$, and $Sr_{2-x}La_xRu_{1-x}Fe_xO_4$ [5–7]. This latter MR component dominates at larger x, e.g., $x = 0.5$ (inset of figure 10), and at 10 K it reaches -70% which is an unprecedented MR value for non-manganite and non-cobaltite perovskites. This phenomenon will be examined in more detail elsewhere.

4. Discussion

According to figures 8 and 9, Zr^{4+} substitution is the least disruptive among the non-magnetic dopants studied here. This is quite unexpected since Zr^{4+} is grossly oversized compared to Ru^{4+}, which should compel RuO_6 octahedron tilting—a highly unfavorable situation according to the first-principles calculation and the band structure theory of Mazin and Singh [2]. Indeed, according to their theory the substitution of undersized Ti^{4+} should have been less disruptive to Stoner FM than Zr^{4+}. Yet contrary to the theoretical prediction, both M and T_C decrease faster upon Ti substitution than upon Zr substitution, as shown in figure 11.

To understand why Zr^{4+} is less disruptive than Ti^{4+}, we propose an electronic explanation based on the fact that the d-electron (t_{2g}^4) energy (E) levels of Ru^{4+} is closer to those (d^0) of Ti^{4+} (higher by $\Delta E = 2$ eV) than Zr^{4+} (ΔE = 4.5 eV) [30]. As a result, there should be a considerable

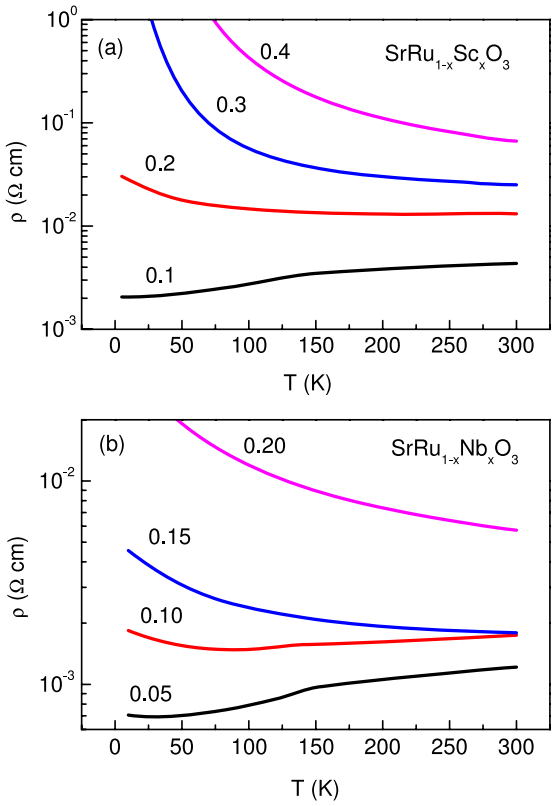

Figure 7. $\rho(T)$ curves for (a) $SrRu_{1-x}Sc_xO_3$ samples, from $x = 0.1$ to 0.4, showing a sign change in the (high temperature) slope at about $x = 0.2$; and (b) $SrRu_{1-x}Nb_xO_3$ samples, from $x = 0.05$ to 0.2, showing a sign change between $x = 0.1$ and 0.15.

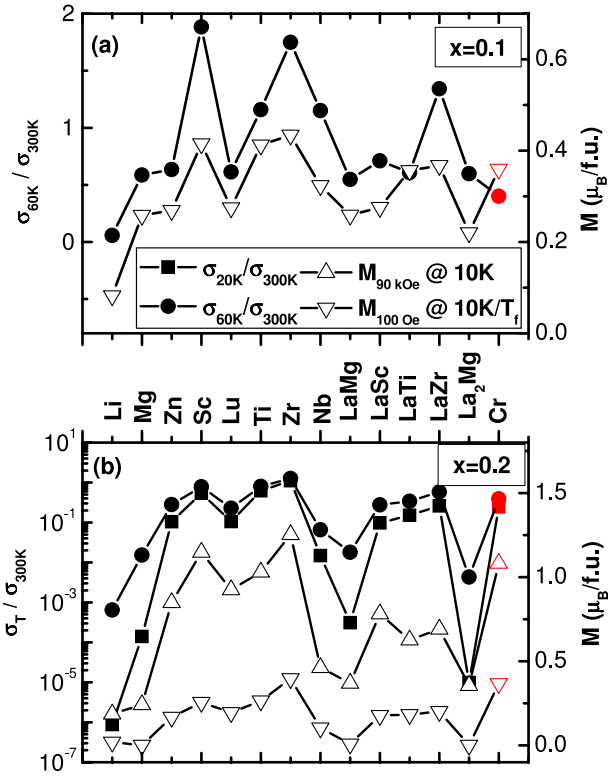

Figure 8. Variation of magnetization at strong field (90 kOe) and weak field (100 Oe) is strongly correlated to normalized conductivity at 20 and 60 K in $SrRuO_3$ with various cation substitutions, listed in the order of nominal valence z of the B'/AB' cation. Same symbols are used in (a) $x = 0.1$ and (b) $x = 0.2$. The data of Cr substitution is shown on the far right for comparison. (See text for the effect of Cr, which is magnetic unlike other dopants shown here.)

probability of resonance scattering of (Ru^{4+}) electrons by Ti^{4+} that would lead to a virtual bound state of Ti^{3+}; this is less likely to occur for Zr^{4+}. Therefore, there is more electron localization under Ti substitution than Zr substitution, which corrupts FM. Interestingly, other than Zr and Ti, the B' that causes the least disruption to σ and M at low x is Sc^{3+}, which has an estimated ΔE about 1.5 eV above Ti^{4+} and thus should rank between Ti^{4+} and Zr^{4+} [31]. This is consistent with figures 8 and 9. Because of charge disorder, however, Sc^{3+} eventually causes a larger disruption than Ti^{4+} at higher x. This is evident from a comparison of the T_C and large-field magnetization under Sc and Ti doping in figure 11: Sc^{3+} and Ti^{4+} have a similar effect at lower x, but at $x = 0.3$, Sc^{3+} lowers the T_C and magnetization more than Ti^{4+} does. The same trend was also confirmed for the 100 Oe $M(T)$ values (data not shown), and we note that Sc substitution also has a slightly lower x_c than Zr and Ti substitutions, see table 1. Following this reasoning, we believe that among all the non-magnetic elements that may possibly enter the B site, Zr^{4+} (and probably Hf^{4+}, which has the same size and an even larger ΔE) should be the least disruptive to the conductivity of $SrRuO_3$. Because Stoner instability rests upon the itinerancy of electrons, it is natural that Zr^{4+} (and Hf^{4+}) is also the least disruptive to FM. As already mentioned in section 1, similar resonance scattering by Fe^{3+} in $SrRuO_3$ causes the magnetic polarization of itinerant electrons near the Fe site resulting in an enhanced magnetic moment in the alloy [5].

The work thus indicates that the Stoner FM in $SrRuO_3$ is quite robust and may withstand considerable B-site substitution (up to 30%) provided the itinerancy of electrons is not severely disrupted. This is despite a myriad of electronic transitions, including superconductivity, observed at low temperatures in perovskite-based ruthenates which suggest an apparent sensitivity of electronic properties to structure variations [32]. Our results are consistent with the literature of A-site substituted $SrRuO_3$ which does not disrupt the Ru–O network; for example, the fact that $Sr_{1-x}Ca_xRuO_3$ is metallic throughout the entire range indicates that Ca hardly disrupts metallicity; therefore, FM is maintained up to $x = 0.8$ in Ca substitution [3]. The finding also sheds light to the effect of magnetic dopants, including Cr. Such dopants are expected to cause spin polarization of electrons to various extent, thus they are intrinsically disruptive to metallicity, hence unfavorable for FM unless there is a strong dopant–Ru or dopant–dopant exchange interaction that is FM. Even for $SrRu_{1-x}Cr_xO_3$, despite its enhanced T_C, it is found $SrRu_{1-x}Cr_xO_3$ ceramics at both $x = 0.1$ and 0.2 actually have a lower normalized conductivity than $SrRu_{1-x}Zr_xO_3$. These data have been included in figure 8 on the far right. (It is also confirmed that M decreases with x in $SrRu_{1-x}Cr_xO_3$, despite the T_C increase, consistent with the finding in the literature [9, 13–20].) Therefore, Cr does cause a disruption to

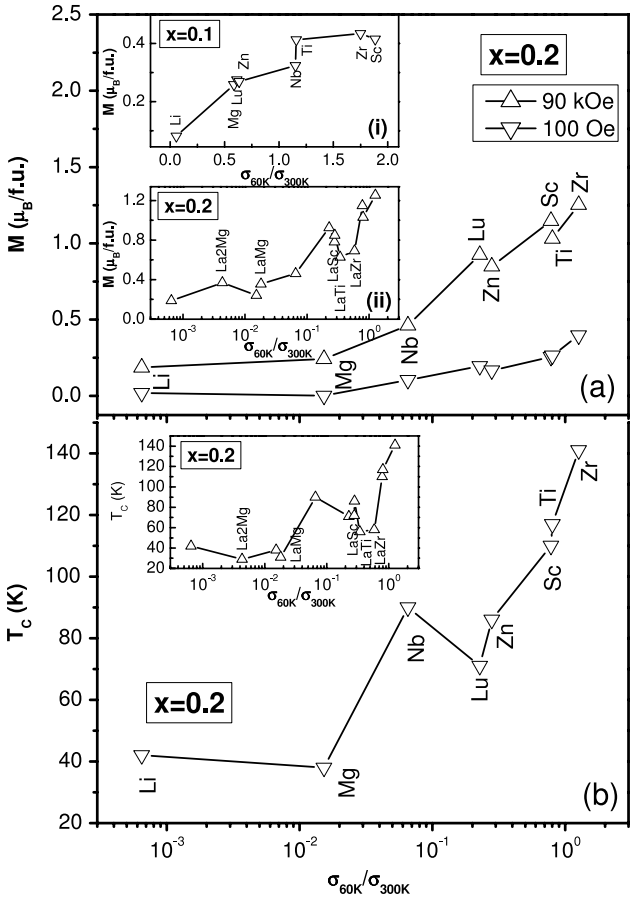

Figure 9. (a) Magnetization at strong field (90 kOe) and weak field (100 Oe) is strongly dependent on normalized conductivity in $SrRuO_3$ alloys, both for B-site substitution at $x = 0.2$ (main panel) and $x = 0.1$ (upper inset), and for mixed A/B-site substitution at $x = 0.2$ (lower inset). (b) Curie temperature T_C versus normalized conductivity at $x = 0.2$, main panel for B-site substitution and inset for mixed A/B-site substitution. Same symbols used in main panel and insets.

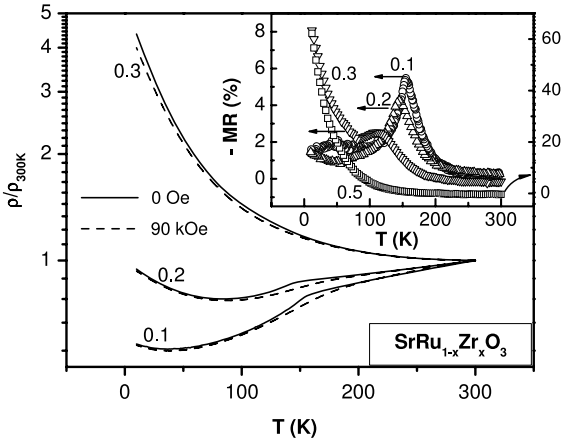

Figure 10. Normalized resistivity of $SrRu_{1-x}Zr_xO_3$ is suppressed by a large field (90 kOe), especially near T_C. Inset: negative magnetoresistance (MR) peaks at T_C; a second MR component that increases with decreasing temperature dominates in the insulating regime at low temperature and large x, reaching -70% at 10 K for $x = 0.5$.

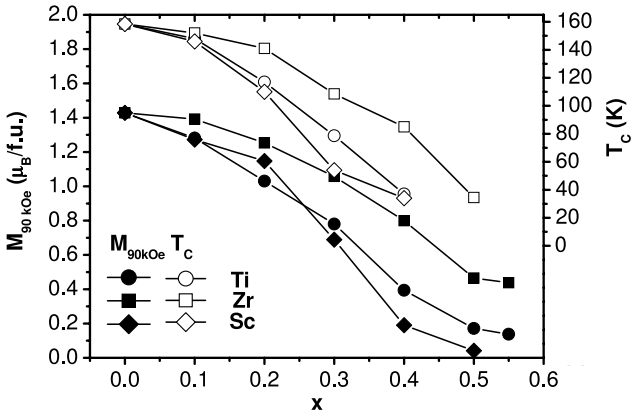

Figure 11. Large-field (90 kOe) magnetization at 10 K and T_C of $SrRu_{1-x}Zr_xO_3$ are higher than those of $SrRu_{1-x}Ti_xO_3$ at all compositions x. Properties of $SrRu_{1-x}Sc_xO_3$ are similarly to $SrRu_{1-x}Ti_xO_3$ at lower x, but lower at higher x.

metallicity, as expected for any magnetic dopant, even though a presumably strong FM exchange interaction of the Cr–Ru pair or the Cr–Cr pair can overcome this disadvantage to raise T_C (but not M).

The strong correlation between FM and electron localization provides a new insight to the dopant effects of $SrRuO_3$. In the past, alloying efforts aiming to enhance the FM of $SrRuO_3$ were mainly designed based on (a) electronic doping considerations attempting to alter the valence of Ru, and (b) lattice distortion considerations attempting to alter the bandwidth, hence DOS, at the E_f. As already mentioned in the section 1, nearly all such efforts instead led to a severe suppression of the FM. We believe one reason for this outcome is electron localization, which depletes the DOS at the E_f, thus suppressing the Stoner instability. The current study of normalized conductivity of itinerant electrons is a sensitive, though non-specific probe of the DOS changes at the E_f. (Normalized conductivity reflects not only carrier concentrations, which may be depleted by electron localization, but also mobility which may be altered without necessarily causing localization.) Direct evidence of the depletion of DOS at the E_f as a result of doping was obtained by photoemission spectroscopy in $Sr(Ru_{1-x}Ti_x)O_3$ [33]. Direct evidence of the depletion of carrier concentrations was also obtained in the same system by optical conductivity, which shows that both Drude-like electron contributions and the plasma edge decrease and eventually vanish as the Ti amount increases [8]. These results are consistent with ours and together they support our finding that the FM of $SrRuO_3$ is strongly correlated to electron itinerancy, just as the metal-to-insulator transition that occurs in all the doped $SrRuO_3$ systems studied here.

As mentioned in [8] and [33], the dopant effects on $SrRuO_3$ can be understood to some extent within the context of the Anderson–Hubbard Hamiltonian which considers a hopping integral t between neighboring sites, an on-site Coulomb energy U, and a random site potential ε. Such a model can explain the decrease of DOS at the E_f due to the destruction of coherent scattering and the quasiparticle peak, hence the suppression of FM in $SrRuO_3$. As the concentration

of dopants increases, there is also an attendant decrease in the normalized t/U due to disorder, which results in a metal-to-insulator transition. A similar argument can be used to rationalize the crossover from the metallic behavior to the correlation insulator behavior as structural disorder increases in $SrRuO_3$, which manifests itself both in magnetism and in low temperature conductivity [29, 34]. The above model is incomplete, however. In the case of Zr/Ti doping, Zr doping creates more randomness in the site potential than Ti doping, yet there is less localization and magnetism disruption caused by Zr doping. This points to a clear need to include resonance scattering into the model: resonance scattering occurs when the (electronic) site potential is well matched, and it has the effect of increasing U/t.

Since $SrRuO_3$ is a common electrode for perovskite-oxide-based thin film devices, the finding that Zr substitution causes the least disruption to conductivity is also of practical utility. In this regard, the simultaneous (oversized) Zr substitution on B site and (undersized) Ca substitution on A site could be advantageous since it can best maintain conductivity and the average unit cell volume at the same time. Our lab experience additionally indicated that sputtering targets of Zr substituted $SrRuO_3$ can be readily sintered to full density whereas $SrRuO_3$ cannot, due to another beneficial effect of Zr on suppressing grain growth and Ru volatility.

4.1. Conclusions

This work demonstrated a strong correlation between the conductivity and Stoner FM in $SrRuO_3$, and that the destruction of FM by non-magnetic cation substitution of Ru is due to electron localization. Among all the non-magnetic cations that enter the B site, Zr^{4+} is the least disruptive to conductivity and FM, because it causes no charge disorder and the least resonance scattering of the d electrons of Ru^{4+}. Such $SrRuO_3$ alloys may be used as conducting electrode for perovskite-oxide-based devices.

Acknowledgments

This work was supported by National Science Foundation of China (Grant No. B010504-20471068), Chinese Postdoctoral Science Foundation and the US National Science Foundation (Grant No. DMR05-20020, 07-05054 and 09-07523).

References

[1] Longo J M, Raccah P and Goodenough J B 1968 *J. Appl. Phys.* **39** 1327
[2] Mazin I I and Singh D J 1997 *Phys. Rev.* B **56** 2556
[3] Cao G, McCall S, Shepard M, Crow J E and Guertin R P 1997 *Phys. Rev.* B **56** 321
[4] He T, Huang Q and Cava R J 2000 *Phys. Rev.* B **63** 024402
[5] Mamchik A and Chen I-W 2004 *Phys. Rev.* B **70** 104409
[6] Mamchik A, Dmowski W, Egami T and Chen I-W 2004 *Phys. Rev.* B **70** 104410
[7] Mamchik A and Chen I-W 2003 *Appl. Phys. Lett.* **82** 613
[8] Kim K W, Lee J S, Noh T W, Lee S R and Char K 2005 *Phys. Rev.* B **71** 125104
[9] Pi L, Maignan A, Retoux R and Raveau B 2002 *J. Phys.: Condens. Matter* **14** 7391
[10] Crandles D A, Reedyk M, Schaeffer R W, Hultgren A E and Schlee R 2002 *Phys. Rev.* B **65** 224407
[11] Bianchi R F, Carrio J A G, Cuffini S L, Mascarenhas Y P and Faria R M 2000 *Phys. Rev.* B **62** 10785
[12] Shuba S, Mamchik A and Chen I-W 2006 *J. Phys.: Condens. Matter* **18** 9215
[13] Han Z H, Budnick J I, Hines W A, Dabrowski B, Kolesnik S and Maxwell I 2005 *J. Phys.: Condens. Matter* **17** 1193
Dabrowski B, Kolesnick S, Chmaissem O, Maxwell T, Avdeev M, Barnes P M and Jogensen J D 2005 *Phys. Rev.* B **72** 054428
[14] Dabrowski B, Kolesnick S, Chmaissem O, Maxwell T, Mais J and Jogensen J D 2006 *Phys. Status Solidi* b **243** 13
Kolesnik S, Yoo Y Z, Chmaissem O, Dabrowski B, Maxwell T, Kimball C W and Genis A P 2006 *J. Appl. Phys.* **99** 08F501
[15] Durairaj V, Chikara S, Lin X N, Douglass A, Cao G, Schlottmann P, Choi E S and Guertin R P 2006 *Phys. Rev.* B **73** 214414
[16] Kasinathan D and Singh D J 2006 *Phys. Rev.* B **74** 195106
[17] Klein Y, Hebert S, Maignan A, Kolesnik S, Maxwell T and Dabrowski B 2006 *Phys. Rev.* B **73** 052412
[18] Williams A J, Gillies A, Attfield J P, Heymann G, Huppertz H, Martinez-Lope M J and Alonso J A 2006 *Phys. Rev.* B **73** 104409
[19] Pietosa J, Dabrowski B, Wisniewski A, Puzniak R, Kiyanagi R, Maxwell T and Jorgensen J D 2008 *Phys. Rev.* B **77** 104410
Rodgers J A, Williams A J, Martinez-Lope M J, Alonso J A and Attfield J P 2008 *Chem. Mater.* **20** 4797
Woods G T, Sanders J, Kolesnik S, Maxwell T, Srikanth H, Dabrowski B, Osofsky M S and Soulen R J Jr 2008 *J. Appl. Phys.* **104** 083701
[20] Hadipour H and Akhavan M 2010 *J. Solid State Chem.* **183** 1678
Wang L, Hua L and Chen L F 2010 *Solid State Commun.* **150** 1069
Ramana E V, Park H W and Jung C U 2010 *IEEE Trans. Magn.* **46** 2228
[21] Clogston A M, Matthias B T, Peter M, Williams H J, Corenzwit E and Sherwood R C 1962 *Phys. Rev.* **125** 541
[22] Oswald A, Zeller R and Dederichs P H 1986 *Phys. Rev. Lett.* **56** 1419
[23] Jaccarino V and Walker L R 1965 *Phys. Rev. Lett.* **15** 258
[24] Eom C B, Van Dover R B, Phillips J M, Werder D J, Marshall J H, Chen C H, Cava R J and Fleming R M 1993 *Appl. Phys. Lett.* **63** 2570
[25] Kim S G, Wang Y-D and Chen I-W 2006 *Appl. Phys. Lett.* **89** 031905
[26] Wang Y, Kim S G and Chen I-W 2008 *Acta Mater.* **56** 5312
[27] Shannon R D 1976 *Acta Crystallogr.* A **32** 751
[28] Allen P B, Berger J, Chauvet O, Forrro L, Jarlborg T, Junod A, Revaz B and Santi G 1996 *Phys. Rev.* B **53** 4393
[29] Klein L, Dodge J S, Ahn C H, Reiner J W, Mieville L, Geballe T H, Beasley M R and Kapitulnik A 1996 *J. Phys.: Condens. Matter* **9** 10111
[30] Lee Y S, Lee J S, Noh T W, Byun D Y, Yoo K S, Yamaura K and Takayama-Muromachi E 2003 *Phys. Rev.* B **67** 113101
[31] Arima T, Tokura Y and Torrance J B 1993 *Phys. Rev.* B **48** 17006
[32] For a review, see Lichtenberg F 2002 *Prog. Solid State Chem.* **30** 103
[33] Kim J, Kim J-Y, Park B-G and Oh S-J 2006 *Phys. Rev.* B **73** 235109
[34] Copogna L, Mackenzie A P, Perry R S, Grigera S A, Galvin L M, Raychaudhuri P, Schofield A J, Alexander C S, Cao G, Julian S R and Maeno Y 2002 *Phys. Rev. Lett.* **88** 076602

Queries for IOP paper 373761

Journal: **JPhysCM**
Author: **W Tong et al**
Short title: **Electron localization and magnetism in** $SrRuO_3$ **with non-magnetic cation substitution**

Page 1

Query 1:

Author: Please check the author names and affiliations carefully.

Query 2:

Author: Amended wording in the abstract and title OK?

Query 3:

Author: Please be aware that the colour figures in this article will only appear in colour in the Web version. If you require colour in the printed journal and have not previously arranged it, please contact the Production Editor now.

Page 8

Query 4:-

Author: Please check the details for any journal references that do not have a blue link as they may contain some incorrect information. Pale purple links are used for references to arXiv e-prints.